Ceramics International 51 (2025) 44306–44316

Contents lists available at ScienceDirect

Ceramics International

journal homepage: www.elsevier.com/locate/ceramint

Recycling biowaste into hydroxyapatite nanorods: a facile route to synthesize antibacterial and antioxidant biomaterials

G. Suresh Kumar [a,*], K. Lalithambigai [b], S. Ranjith Priyan [c], Nguyen Van Minh [d,e,**], M. Hariprasath [c], G. Dineshkumar [c], Srinivasan Ramalingam [f,***], Raji Atchudan [g,h,****], Mohd Shkir [i]

[a] Department of Physics, PSG College of Arts & Science, Coimbatore, 641014, Tamil Nadu, India
[b] Department of Physics, K.S.R College of Engineering, Tiruchengode, 637215, Namakkal, Tamil Nadu, India
[c] Department of Physics, K.S. Rangasamy College of Arts and Science (Autonomous), Tiruchengode, 637215, Namakkal, Tamil Nadu, India
[d] Institute of Research and Development, Duy Tan University, Da Nang, 550000, Viet Nam
[e] School of Engineering & Technology, Duy Tan University, Da Nang, 550000, Viet Nam
[f] Department of Horticulture & Life Science, Yeungnam University, Gyeongsan, Gyeongsangbuk-do, 38541, Republic of Korea
[g] Department of Chemistry, Saveetha School of Engineering, Saveetha Institute of Medical and Technical Sciences, Chennai, 602105, Tamil Nadu, India
[h] School of Chemical Engineering, Yeungnam University, Gyeongsan, 38541, Gyeongsangbuk-do, Republic of Korea
[i] Department of Physics, College of Science, King Khalid University, PO Box 960, Abha, 61421, Saudi Arabia

ARTICLE INFO

Handling Editor: Dr P. Vincenzini

Keywords:
Biowaste
Hydroxyapatite
Nanorods
Antibacterial
Antioxidant
Cell viability

ABSTRACT

In this study, we have reported the sustainable synthesis of hydroxyapatite (HAp) nanorods using biowaste materials such as sea shells and *Citrus sinensis/Punica granatum* fruit peel, as calcium and templating agents, respectively. The hydrothermal method was employed to prepare HAp nanorods with uniform size and shape. XRD, FTIR, SAED, HRTEM, and thermogravimetric analyses confirmed the formation of polycrystalline HAp with rod-like morphology. The antibacterial activity of the HAp nanorods was evaluated against *S. aureus and E. coli*, while the antioxidant activity was assessed using the DPPH method. The incorporation of *Citrus sinensis* and *Punica granatum* fruit peel extracts into the synthesis process imparted antibacterial and antioxidant properties to the HAp nanorods efficiently. The obtained results revealed that the HAp nanorods exhibited concentration-dependent antibacterial and antioxidant activities. Moreover, *Citrus sinensis* fruit peel extract-mediated HAp shows better antibacterial and antioxidant activities than *Punica granatum* fruit peel extract-mediated HAp. Moreover, MTT assay and fluorescence-based live/dead staining demonstrated excellent biocompatibility of the synthesized HAp nanorods with MG63 cells, confirming their suitability for biomedical applications. This approach has the potential to obtain functional biomaterials while simultaneously promoting waste valorization and environmental sustainability.

1. Introduction

Current biomaterials research relies on nanotechnology to address the limitations of bulk materials. Nanoscale materials exhibit unique properties due to quantum confinement effects and exceptional surface area [1–3]. Among the variety of biomaterials available today, nanostructured hydroxyapatite (HAp) received great consideration for dental and orthopedic applications owing to its resemblance with the mineral component of calcified tissues [4]. Also, nanostructured HAp exhibits excellent biocompatibility, bioactivity, and osteoconductivity [3,4]. The particle size and shape of nanostructured HAp have a major impact on its suitability for drug delivery, coatings on metallic implants,

* Corresponding author. Department of Physics, PSG College of Arts & Science, Coimbatore, 641014, Tamil Nadu, India.
** Corresponding author. Institute of Research and Development, Duy Tan University, Da Nang, 550000, Viet Nam.
*** Corresponding author. Department of Horticulture & Life Science, Yeungnam University, Gyeongsan, Gyeongsangbuk-do, 38541, Republic of Korea.
**** Corresponding author. Department of Chemistry, Saveetha School of Engineering, Saveetha Institute of Medical and Technical Sciences, Chennai, 602105, Tamil Nadu, India.
E-mail addresses: gsureshkumar1986@gmail.com (G.S. Kumar), nguyenvanminh15@duytan.edu.vn (N. Van Minh), sribt27@gmail.com (S. Ramalingam), atchudanr@yu.ac.kr (R. Atchudan).

https://doi.org/10.1016/j.ceramint.2025.07.161
Received 14 September 2024; Received in revised form 30 June 2025; Accepted 13 July 2025
Available online 14 July 2025

and making tissue engineering scaffolds. Hence, different methods have been explored to synthesize nanostructured HAp with various morphologies [4,5]. Moreover, a new technique to improve the properties of nanostructured HAp may be developed by combining two or more methods [5,6].

Bacterial infections on implant surfaces are a major issue in orthopedic surgery because they often result in implant failure and need further surgery [7]. Hence, the functionalization of biomaterials with antimicrobials to increase their efficacy in treating post-implant infections has been the subject of much investigation in recent years [8,9]. A fascinating new age of research has been opened by the many studies that have shown the antibacterial and antioxidant properties of metal nanoparticles made via green synthesis from plant extracts [10,11]. Therefore, HAp nanoparticles synthesized sustainably utilizing plant extract as the solvent might potentially possess antibacterial and antioxidant properties [12,13]. Unfortunately, uncontrolled nucleation makes green synthesis a major challenge when trying to synthesize HAp with a well-defined shape and size. Additionally, green synthesis is a time-consuming method with limited yield and repeatability [12,13]. On the other hand, well-crystallized and dispersed HAp nanoparticles with high purity may be achieved effectively using the hydrothermal technique [4,14]. The key issue with the hydrothermal process, however, is the inclusion of specific compounds as chelating agents to regulate the particle size and shape [14]. Phytochemicals in the plant extracts can control morphology and provide intrinsic antibacterial and antioxidant properties [12,13]. By combining green synthesis with a hydrothermal process, it is now possible to synthesize well-defined HAp nanostructures with inherent antibacterial and antioxidant characteristics [13].

The possible uses of HAp nanoparticles derived from biowaste have been extensively documented in the literature [5,15–18]. This process improves material performance and sustainability while lowering environmental waste and producing HAp with desired properties for biomedical applications [15,19,20]. Sea shells are one of the best biosources to employ as a precursor for HAp synthesis among the many calcium-rich biowastes since they contain 95–99 % calcium carbonate (aragonite) [21,22]. Fernández-Penas et al. synthesized HAp nanoparticles using sea shells as a calcium source with enhanced osteoinductive properties for biomedical applications [21]. Similarly, Agalya et al. synthesized antibacterial HAp by doping with silver ions using sea shells with enhanced mechanical properties [23]. Moreover, to control the HAp particle size and shape, biowaste-derived phytochemical extracts have been widely used [12,13]. For example, Kumar et al. described a biogenic method to prepare HAp nanorods using eggshell biowaste as the calcium precursor and *Curcuma longa tuber* extract as the solvent [16]. This novel approach demonstrated an economically feasible technique for producing HAp nanorods by using waste materials and natural components. Likewise, Ali et al. used the microwave-assisted hydrothermal process to develop homogenous HAp nanorods deploying licorice root extract as a template [24]. *Citrus sinensis* fruit peel is referred to as a biowaste in citrus processing industries even though it contains abundant bioactive phytochemicals such as flavonoids, polyphenols, and vitamin C [25,26]. Likewise, *Punica granatum* peel is a type of agricultural and food waste that contains a lot of beneficial substances, including polyphenols, vitamins, dietary fiber, and antioxidants which possess potent pharmaceutical properties [27]. Hence, the present investigation is aimed at the controlled synthesis of HAp nanorods by the hydrothermal method by employing seashell as the calcium source and *Citrus sinensis/Punica granatum* fruit peel extract as natural templating for controlling morphology and incorporating intrinsic antibacterial and antioxidant activity to HAp nanorods for biomedical applications. While the individual use of seashells as a calcium source and fruit peels as templating agents has been reported, our work introduces an integrated and one-pot hydrothermal synthesis approach where both nanostructuring (rod-like morphology) and biofunctionalization (antibacterial and antioxidant properties) are achieved simultaneously using biowaste-derived precursors—without requiring additional dopants, surface modifiers, or post-synthesis treatments. This dual-functionality incorporation during synthesis, particularly using *Citrus sinensis* and *Punica granatum* peels, directly into the HAp crystal structure and surface, imparts enhanced characteristics in a simplified, sustainable, and scalable route. Furthermore, the comparative evaluation of two different fruit peel extracts under identical synthesis conditions to optimize biological performance has not been reported before, to the best of our knowledge. Thus, the novelty lies in this concurrent valorization of two distinct types of biowaste to fabricate multifunctional nanorods in a single step, making it a practically viable and eco-conscious strategy. The use of biowaste materials like sea shells and fruit peels can promote sustainability and leverage their beneficial trace elements and bioactive compounds, improving the overall functionality of the HAp nanorods.

2. Experimental procedure

2.1. Materials

Sodium hydroxide (NaOH) solution, disodium hydrogen phosphate (Na_2HPO_4), hydrochloric acid (HCl), *Citrus sinensis* fruit peel, *Punica granatum* fruit peel, and sea shell, were used for this investigation. Analar-grade chemicals without any further processing were used.

2.2. Synthesis of HAp nanorods

The *Citrus sinensis* and *Punica granatum* fruit peel were first harvested separately and dehydrated at ambient temperature for three days. The dehydrated peel was then finely pulverized using an electric mixer. Next, 10 g of peel powder was immersed in 200 mL of distilled water separately and heated for 2 h at 150 °C under continuous mixing. After cooling, the extract was filtered and used to prepare calcium and phosphate precursors. Then, sea shells were collected, cleaned, and dehydrated at 110 °C for 8 h in a vacuum oven. Afterwards, they were pulverized into a powder form using a mortar and pestle. Next, 1M calcium precursor ($CaCl_2$) was prepared by dissolving 10 g of seashell powder in 2M HCl (10 mL) followed by 40 mL of distilled water. Seashell powder ($CaCO_3$) and HCl react as follows [16].

$$CaCO_3 + 2HCl \rightarrow CaCl_2 + H_2O + CO_2\uparrow$$

Then, the phosphate precursor solution was prepared by dissolving 0.6 M Na_2HPO_4 in 50 mL distilled water. Next, the prepared calcium and phosphate solutions were added one by one slowly into 100 mL of prepared peel extract under constant stirring. Consequently, NaOH solution was used to raise the pH of the reaction mixture to 11. The HAp precipitate was formed according to the below chemical reaction [28].

$$10CaCl_2 + 6Na_2HPO_4 + 8NaOH \rightarrow Ca_{10}(PO_4)_6(OH) + 6H_2O + 20NaCl$$

The resulting reaction mixture was subjected to hydrothermal treatment at 120 °C for 10 h. Then, the centrifugation and washing process were employed to remove the by-product from the resulting reaction mixture. Finally, the resulting precipitate was subjected to heat treatment at 100 °C for 10 h to get the final product. It is noted that samples were prepared separately using *Citrus sinensis* and *Punica granatum* fruit peel extract as the templating agent using the above procedure and the obtained sample was named as CS-HAp and PG-HAp. Fig. 1 shows the schematic of the process involved in the synthesis of HAp nanorods using *Citrus sinensis* and *Punica granatum* fruit peel extract and sea shell calcium source.

2.3. Characterization

X-ray diffraction (XRD) data in the 2θ range of 20–60° were obtained using a Bruker D8 advance powder X-ray diffractometer that was

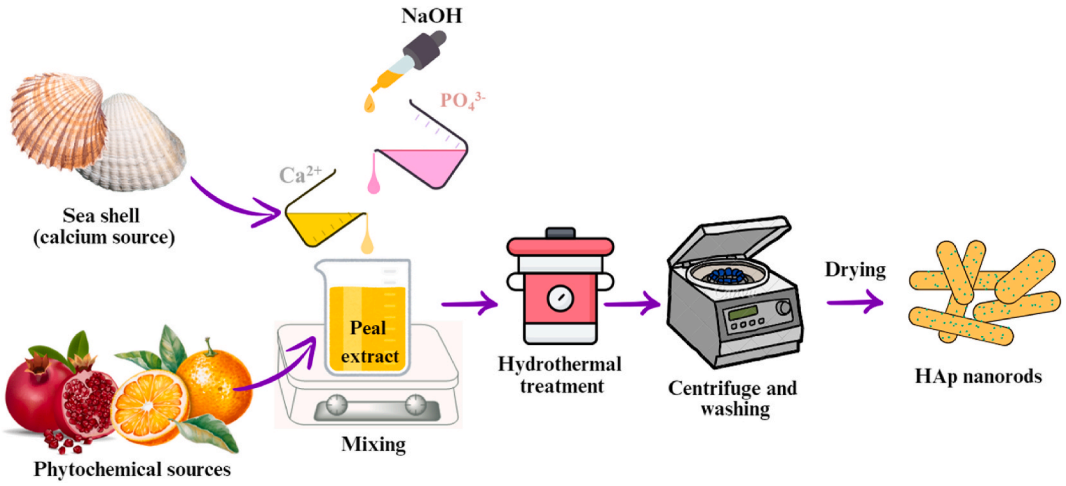

Fig. 1. The schematic presentation of the process involved in the hydrothermal synthesis of HAp nanorods using *Citrus sinensis* and *Punica granatum* fruit peel extract and sea shell calcium source.

operated at current and voltage settings of 30 mA and 40 kV using Cu-Kα monochromatic radiation (1.5406 Å). The lattice constants for hexagonal structured HAp were calculated using lattice spacing (*d*) and Miller's plane (*hkl*) value from the XRD pattern via the below relation [29].

$$\frac{1}{d^2}=\frac{4\left(h^2+hk+k^2\right)}{3a^2}+\frac{l^2}{c^2}$$

Moreover, the unit cell volume (*V*) for hexagonal structured HAp was calculated using the below relation.

$$V=\frac{\sqrt{3}}{2}\times a^2\times c^2$$

The KBr method was used with a Bruker Tensor 27 FT-IR analyzer to get the FTIR spectra of the prepared samples in the 400–4000 cm^{-1} range. A single droplet of sample dispersion prepared with ethyl alcohol was positioned copper grid in a JEOL JEM 2100 high-resolution transmission electron microscope (HRTEM) to analyze the size, shape, and lattice structure of the samples. NETZSCH thermal analyzer (Model: STA 449F1 Jupiter®) was used to perform thermogravimetric tracing (Heating rate: 10 °C/min; Temperature range:30–1000 °C) of the prepared samples.

2.4. Antibacterial activity test

Bacteria that cause bone infections were the targets of the antibacterial activity tests. The well-diffusion assay was used to determine the antibacterial activity of the produced samples against *S. aureus and E. coli* [30]. The bacterial inoculum suspension was made by first preparing nutrient broth, inoculating *S. aureus and E. coli* separately, and then incubating them at 37 °C for 8 h. Each bacterial solution was then spread out evenly on the agar plates' surface. After that, a 6 mm diameter well was cut out of the agar plates and then filled with different amounts of the samples. Chloro tetrocycle (30 μg concentration)- CT-30 was used as control. The plates were incubated for 24 h at 37 °C. After the time for growth, the pictures were taken and used to pattern the inhibiting zone of micro-organisms.

Acridine Orange/Propidium Iodide (AO/PI) dual-staining was employed to assess the viability of bacterial cells after treatment with the tested sample [31]. *E. coli* and *S. aureus* cultures were grown to the late log-phase, harvested by centrifugation, and washed thoroughly with 0.85 % NaCl to remove growth media. The bacterial suspension was then incubated with the test sample for 24 h at 37 °C. After treatment, cells were centrifuged and washed to remove residual sample, followed by staining with a 1:1 mixture of Acridine Orange and Propidium Iodide (2–3 μL/mL) for 15 min in the dark. Fluorescence microscopy was performed, where live (green, AO-stained) and dead (red, PI-stained) cells were imaged to evaluate the antimicrobial efficacy of the tested material.

2.5. Antioxidant activity

The DPPH (2,2-diphenyl-1-picrylhydrazyl) assay was used to analyze the antioxidant activity of the prepared samples [32]. The analysis of antioxidant activity is based on the reduction of the DPPH radical by the sample. This technique involves analyzing a color shift from violet to yellow that occurs when the radical is neutralized. The dose-dependent activity antioxidant activity was examined using the prepared samples with different concentrations. DPPH was initially dissolved in methanol at a concentration of 0.3 mM. Next, the DPPH solution (10 mL) was transferred to test tubes and then prepared HAp samples were added at different concentrations. The test tubes were then kept in darkness for 1 h. Subsequently, the absorbance of the tested DPHH solution was determined using a UV spectrophotometer. The antioxidant activity was calculated from absorbance using the below relation [33].

$$\text{DPPH }(\%)=\frac{Control-Test}{Control}\times 100\%$$

2.6. MTT assay

The MTT assay is a colorimetric assay mostly used in evaluating cell viability, and cytotoxicity by measuring cellular metabolic activity [34,35]. MTT assay is based on the enzymatic reduction of a yellow tetrazolium salt MTT into insoluble purple formazan crystals by mitochondrial enzymes in metabolically active cells. To check the samples for cytotoxicity, MG-63 osteoblast cells were seeded into a 96-well plate at a density of 10,000 cells/well in DMEM for 24 h standard culture conditions (37 °C, 5 % CO_2) in a CO_2 incubator for attachment and stabilization and then treated with for different HAp concentrations ranging from 50 to 200 μg/mL, while untreated cells were maintained as controls. After 24 h, cells were washed twice with phosphate-buffered saline (PBS) to remove residual HAp nanoparticles. This allowed the metabolically active cells to reduce the MTT to insoluble formazan crystals. Subsequently, the MTT solution was removed and 150 μl of dimethyl sulfoxide (DMSO) was added to each well to dissolve the formazan crystals. The plate was then shaken gently for 15 min to ensure total dissolution. The absorbance values were measured at 570 nm using an ELISA reader Mindray MR-96 (Mindray, Nanshan, China) and cell viability was calculated as a percentage against the untreated control

cells.

2.7. Live/dead cell staining by fluorescence assay

Calcein AM is a cell-permeable dye which transforms intracellular esterases of living cells into green fluorescence, whereas Propidium Iodide is a membrane-impermeable dye which stains nucleic acids in the dead cells by emitting red fluorescence [36]. MG-63 osteoblast cells were seeded for 24 h under standard culture conditions (37 °C, 5 % CO_2). Then, cultured cells were treated with the prepared HAp samples at different concentrations ranging from 50 to 200 μg/mL, whereas untreated cells were maintained as controls. After 24 h of treatment, the cells were washed using PBS to eliminate residual HAp nanoparticles. Then staining solution with Calcein AM (2 μM) and PI (1 μg/mL) were added to the cells followed by incubation for 15–30 min at 37 °C in dark conditions. Then, stained cells were visualized under an Olympus fluorescent microscope (CKX53, OLYMPUS, Japan), where fluoresce live cells were green and dead cells red.

2.8. Statistical analysis

All experiments were performed in triplicates, and the results are presented as mean ± standard deviation (SD). The data were statistically analyzed using the Statistical Package for Social Sciences (SPSS) software (version 16.0; SPSS Inc., USA). Differences between the control and treated groups were evaluated using a one-way analysis of variance (ANOVA), followed by Tukey's post hoc test for multiple group comparisons. A p-value of less than 0.05 ($p < 0.05$) was considered statistically significant. Error bars representing the standard deviation were included in the respective figures to indicate variability within the data.

3. Results and discussion

Fig. 2 (a) revealed the XRD patterns of the CS-HAp and PG-HAp samples. The measured angle of diffraction peaks closely matched the JCPDS data for HAp (File No. 09–0432) in both samples, indicating the formation crystalline phase as HAp with a hexagonal structure. A substantial peak resembling bone apatite mineral could be seen in the 31–34° area. This peak is ascribed to diffraction from the (211), (1 1 2), and (300) Miller's planes of HAp. The lattice constant and unit cell volume of the hexagonal structured HAp phase in CS-HAp and PG-HAp samples were calculated and provided in Table 1. There was a noticeable difference in the lattice constants between the two samples. Furthermore, the CS-HAp has an increased unit cell size in comparison to the PG-HAp. This demonstrates that the biomolecules present in *Citrus sinensis* extracts interact with calcium ions efficiently and regulate the growth of HAp crystals during synthesis, hence modifying the unit cell characteristics. The variation in the lattice parameter could suggest the interaction between HAp ions and phytochemicals present in the peel extracts, as supported by Kumar et al. [28].

Fig. 2(b) revealed the FT-IR spectra of the prepared HAp samples and raw peel extracts. Both HAp samples revealed the vibrations of PO_4^{3-} and OH^- ions of hexagonal structured HAp. The peaks at 472 cm^{-1}, 564 cm^{-1}, 602 cm^{-1}, 962 cm^{-1}, and 1024 cm^{-1} were attributed to the tetrahedral vibrational modes of the PO_4^{3-} groups of HAp [37,38]. The peaks at 628 cm^{-1} and 3570 cm^{-1} were standard to characteristic vibrational modes of OH^- ions in the HAp structure [37]. In the FTIR spectra of both samples, a wide band spanning from 2600 to 3700 cm^{-1}

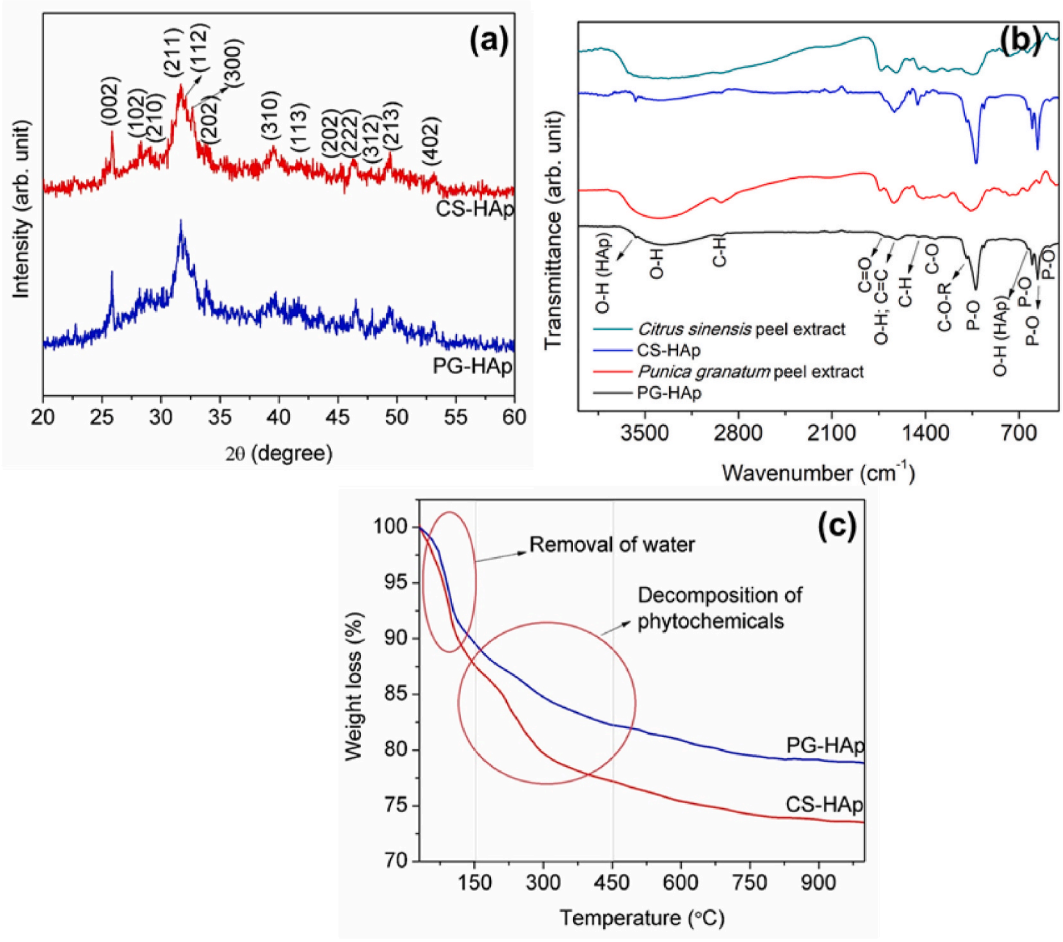

Fig. 2. (a) XRD patterns (b) FTIR spectrum and (c) Thermogravimetric trace of the samples.

Table 1
The calculated lattice constants and unit cell volume of the hexagonal structured HAp phase in CS-HAp and PG-HAp samples.

Sample	Lattice constants (Å)		Unit cell volume (Å^3)	Lattice distortion c/a
	a = b	c		
CS-HAp	9.4161 ± 0.003	6.8791 ± 0.005	528.22 ± 0.07	0.7305 ± 0.0008
PG-HAp	9.3784 ± 0.002	6.8990 ± 0.003	525.51 ± 0.06	0.7356 ± 0.0009

and a peak at 1630 cm^{-1} was found, which represents the existence of lattice water molecules [28,37]. FTIR spectrum of raw peel extracts revealed the fingerprints of phytochemicals. A prominent peak at 1080 cm^{-1} indicates C-O-H interactions of alcohols and esters. The distinctive peaks at 2929 cm^{-1} and 1447 m^{-1} belong to C-H stretching and bending vibrations related to aliphatic chains (-CH_2 and -CH_3) [39,40]. A peak at 1711 cm^{-1} indicates the presence of a carbonyl group, which was found in esters [39–42]. Further, the band at 1632 cm^{-1} is presumably connected to C=C stretching in aliphatic and aromatic compounds. Comparision of FTIR spectrum of HAp samples and peel extracts confirm the existence of phytochemicals in the prepared HApsamples.

The TGA curve of CS-HAp and PG-HAp samples is shown in Fig. 2(c). It shows the weight loss of the prepared samples as a function of temperature. It revealed around 10–13 % weight loss in both samples up to 150 °C [43] which is owing to dehydration of the samples. Then, a weight loss of around 10 % for CS-HAp and 7 % for PG-HAp was detected between 150 and 450 °C representing the decomposition of phytochemicals [44]. TGA results confirm the presence of phytochemicals and water content in CS-HAp and PG-HAp samples and correlate well with FTIR analysis.

HRTEM pictures shown in Fig. 3 (a&b) and (d&e) provide evidence of the existence of HAp nanorods with 10–20 nm in width and 80–150

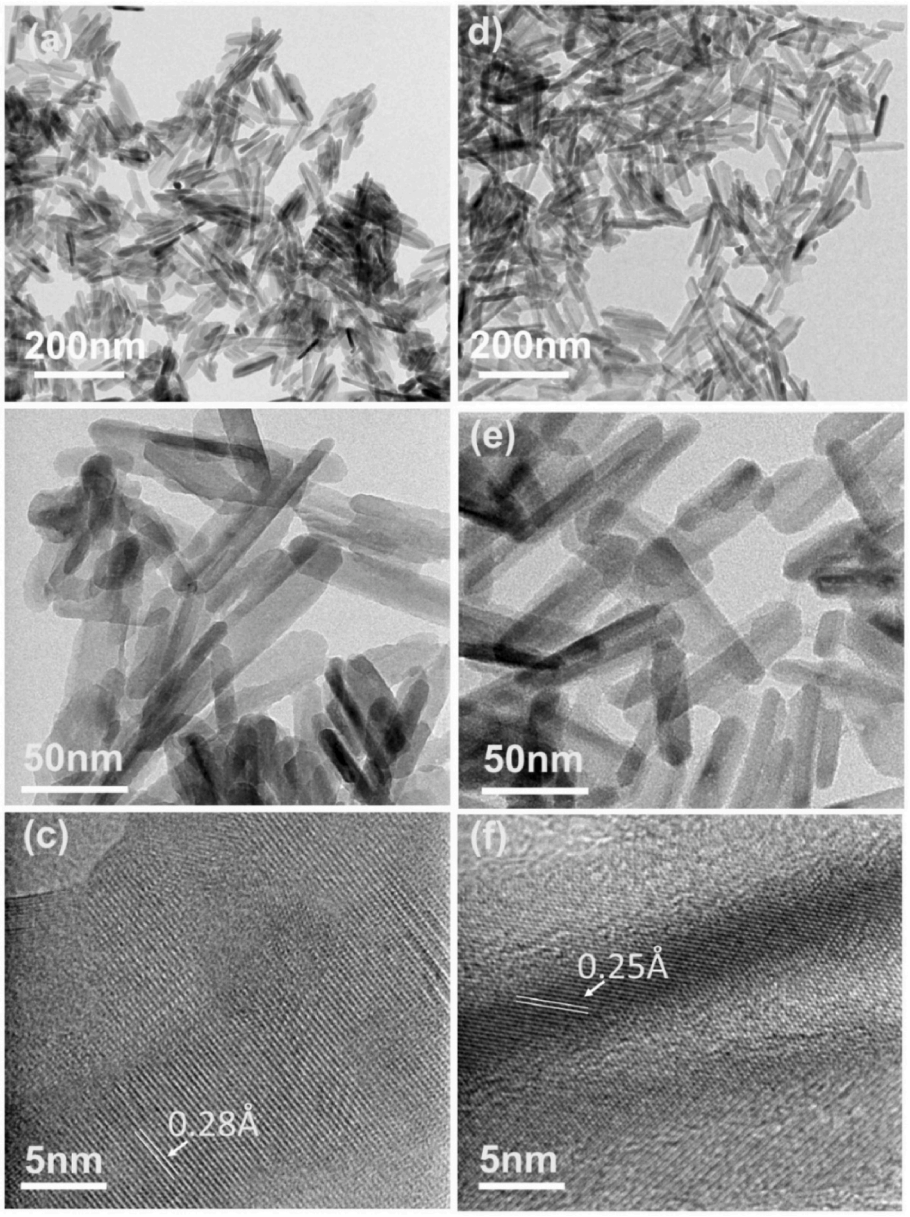

Fig. 3. HRTEM images of (a–c) CS-HAp and (d–f) PG-HAp samples.

nm in length in CS-HAp samples, whereas PG-HAp samples contain nanorods that are 20–30 nm wide and 100–200 nm long. Further, the nanorods in PG-HAp have relatively uniform size distribution with less degree of agglomeration than CS-HAp. This difference may be attributed to the higher presence of phytochemicals in the CS-HAp sample, as indicated by the FTIR and TGA results. HRTEM images of CS-HAp and PG-HAp samples at high magnification are revealed in Fig. 3 (c) & (f) and show a clear periodic lattice structure which is one of the characteristics of a crystalline material [45]. The regular arrangement of atoms in the crystal lattice was seen by bright and dark spots. The lattice spacing was found to be 0.28 Å for CS-HAp whereas 0.25 Å for PG-HAp. In certain areas, there are noticeable changes in the orientation of the crystal lattice, indicating the probable existence of defects within the crystal lattice [45].

The phytochemicals present in the plant extract play a crucial role in facilitating the development of HAp nanorod [15,16,21]. *Citrus sinensis* and *Punica granatum* peel extracts are rich in bioactive compounds like polyphenols, flavonoids, and organic acids [46,47]. These compounds act as chelating, reducing, and capping agents, stabilizing calcium and phosphate precursors (e.g., calcium nitrate and diammonium hydrogen phosphate) while directing controlled nucleation [34]. During the hydrothermal process, the reaction mixture is heated in a sealed autoclave at elevated temperatures and pressures, promoting crystallization and anisotropic one-dimensional growth into nanorods. The bioactive molecules selectively interact with specific crystal facets of HAp, aiding in morphology control [13]. Kalaiselvi et al. reported a novel microwave-assisted green synthesis approach for synthesizing HAp nanorods using *Moringa oleifera* flower extract [48]. Similarly, Kumar et al. developed HAp nanorods using Curcuma longa tuber extract as a soft template and eggshell as a calcium source via a sol-gel approach [16]. Also, they synthesized HAp nanorods using *Coccinia grandis* and *Azadirachta indica* through a green approach [28]. The above studies indicate that the phytochemicals present in the plant extract have the potential to facilitate the hydrolysis of precursors and the subsequent growth of HAp nanorods. However, most of the studies show highly agglomerated nanorods with inhomogeneity [13,28]. In the present study, we have obtained well-defined HAp nanorod with uniformity. It revealed phytochemicals present in the Citrus sinensis and Punica granatum fruit peel extracts are more favourable for the hydrothermal synthesis of homogeneous HAp nanorods.

The SAED pattern of both samples shown in Fig. 4 revealed a series of concentric rings that confirm polycrystalline characteristics [45]. In other words, the SAED pattern indicates that both samples are composed of numerous small crystallites that are randomly oriented. The positions of the rings can be indexed to (002), (211), (300), (202), and (310) planes of hexagonal structured HAp which is well matched with XRD results.

HAp-based materials with antibacterial activity are commonly required in biomedical applications, such as bone replacement and repair [13]. However, pure HAp does not possess inherent antibacterial properties [28]. Fig. 5 revealed the antibacterial activity of CS-HAp and PG-HAp samples against *S. aureus and E. coli.* CS-HAp and PG-HAp samples exhibit a large zone of inhibition compared to the control. Further, Table 2 summarizes the zone of inhibition for each bacterial strain and dose. As the concentration of the sample increased, both bacterial strains revealed an increased zone of inhibition. This suggests that the antibacterial action of CS-HAp and PG-HAp samples against *S. aureus and E. coli* is concentration-dependent. Furthermore, the zones of inhibition may fluctuate for different bacterial strains due to variations in their cell wall structures and levels of sensitivity to different phytochemicals present in the CS-HAp and PG-HAp samples. An AO/PI dual-staining methodology was utilized in fluorescence microscopy to determine the bacterial cell viability treated with samples. Fig. S1 depict a different fluorescence scenario, wherein green cells have intact membranes and are stained by Acridine Orange, while red cells are those that lost their membrane and were stained by Propidium Iodide. Both green and red signals represent a mixed population, suggesting a partial membrane disruption reflecting the antimicrobial activity of the sample under test. The phytochemicals present in the peel extracts can accumulate with HAp nanoparticles during the synthesis process and provide inherent antibacterial characteristics, making them potentially antibacterial materials [13]. Gopi et al. have successfully synthesized the HAp nanoparticles employing Opuntia ficus indica fruit peel as a soft template and observed intrinsic antimicrobial activity against different micro-organisms [49]. Umesh et al. found that phytochemicals present in *piper betel* extract are useful in incorporating antimicrobial properties into HAp nanoparticles [50]. Also, Ragunath et al., HAp nanoparticles with antibacterial activity using *Wrightia tinctoria* through green synthesis [51]. Likewise, *Moringa oleifer* [48], *Azardirachta Indica, Coccina granadis* [28] and *Curcuma longa* plant [16] extracts were found to offer intrinsic antibacterial activity to HAp nanoparticles efficiently. It is well known that the phytochemicals present in the *Citrus sinensis* and *Punica granatum* fruit peel extract can inhibit the growth of bacteria by different mechanisms including damaging bacterial membranes, inhibiting key bacterial enzymes, reducing DNA and protein synthesis and by ROS generation [52–54]. Fig. 6 revealed the different pathways which are responsible for the effectiveness of HAp nanorods in inhibiting bacterial growth. These actions eventually result in an inhibition of bacterial growth or the death of bacterial cells. The efficacy of various phytochemicals against different bacterial strains might vary owing to the intricate nature of bacterial resistance mechanisms [55].

Fig. 7 shows the antioxidant activity of CS-HAp and PG-HAp samples

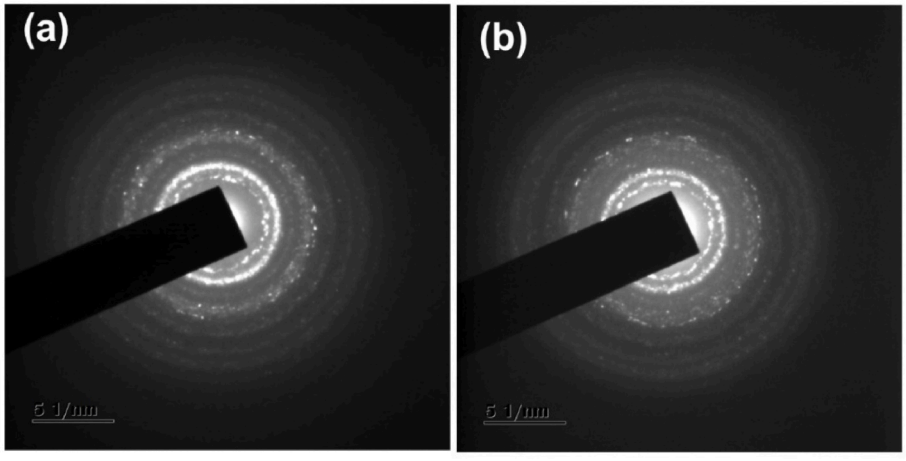

Fig. 4. SAED images of (a) CS-HAp and (b) PG-HAp samples.

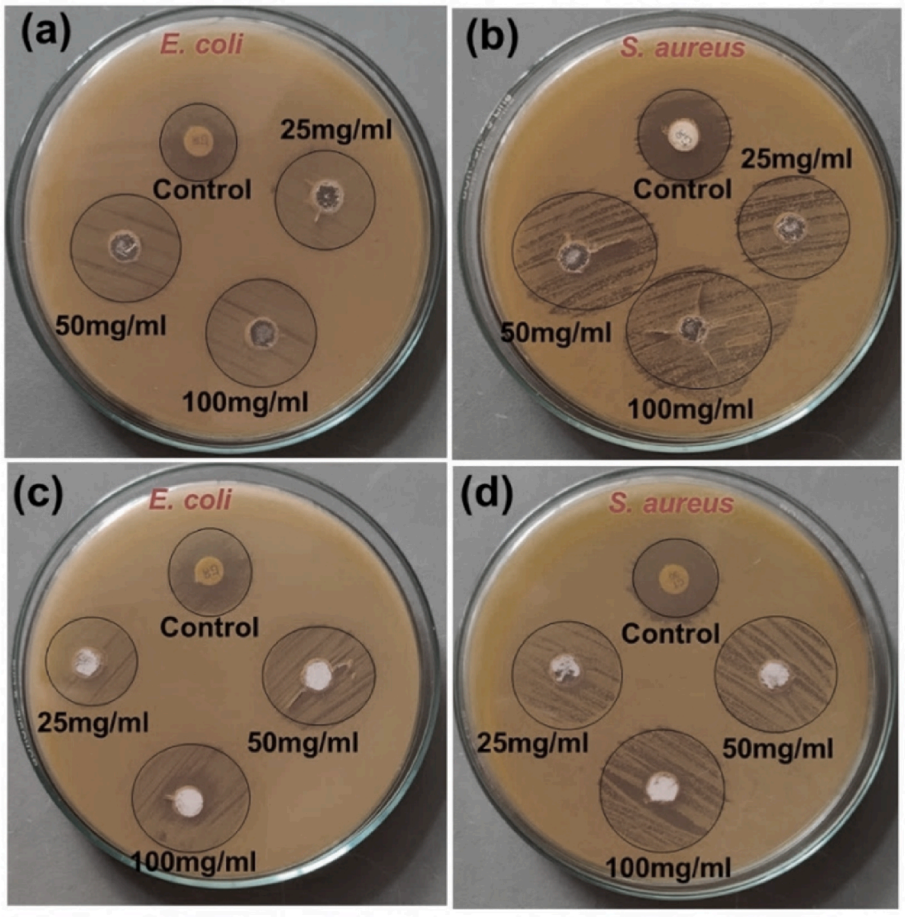

Fig. 5. Antibacterial activity of (a,b) CS-HAp and (c,d) PG-HAp samples against *S. aureus and E. coli* with 25 mg/mL, 50 mg/mL &100 mg/mL. Chloro tetrocycle with 30 μg/mL was used as control.

Table 2
Summary of inhibition zone diameters (mm) for different bacterial strains treated with varying concentrations of CS-HAp and PG-HAp samples, compared with the standard antibiotic control, Chlortetracycline (30 μg) – CT-30.

Sample	*E. coli (mm)*				*S. aureus (mm)*			
	Control (CT30)	25 mg/mL	50 mg/mL	100 mg/mL	Control (CT30)	25 mg/mL	50 mg/mL	100 mg/mL
CS-HAp	17 ± 01	22 ± 03	25 ± 04	26 ± 03	20 ± 02	25 ± 04	30 ± 08	33 ± 06
PG-HAp	18 ± 03	20 ± 04	24 ± 06	25 ± 05	19 ± 02	24 ± 03	26 ± 01	30 ± 02

evaluated by the DPPH method. CS-HAp samples had radical scavenging activities of 77 % (25 mg), 84 % (50 mg), 89 % (75 mg), and 95 % (100 mg) while PG-HAp samples had radical scavenging activities of 58 % (25 mg), 69 % (50 mg), 75 % (75 mg), and 84 % (100 mg). The obtained results revealed that CS-HAp samples exhibited consistently higher antioxidant activity than PG-HAp samples for all concentrations which may be due to different bioactive compounds present in the respective HAp samples. *Citrus sinensis* peel contains flavonoids, phenolic acids, and ascorbic acid whereas *Punica granatum* fruit peel is rich in ellagitannins, flavonoids, and phenolic acids [25–27,52,55]. The phytochemicals present in both extracts are responsible for the observed antioxidant activity of CS-HAp and PG-HAp samples. The phytochemicals present in *Citrus sinensis* and *Punica granatum* fruit peel are well-known for their strong antioxidant properties [25,27]. Therefore, the inherent attributes of phytochemicals in peel extracts enable HAp nanorods to successfully eliminate and neutralize reactive oxygen species (ROS) and free radicals, which are crucial in preventing oxidative stress-related harm in biological systems [56]. They can contribute to primary tissue health by controlling cellular redox signaling pathways, which help shield cells from oxidative damage.

The superior performance of CS-HAp in antibiosis and ROS scavenging compared to PG-HAp can be attributed to the higher concentration of bioactive phytochemicals in *Citrus sinensis peel* extract. *Citrus sinensis* peel contains a diverse range of bioactive compounds, such as alkaloids, flavonoids, phenols, saponins, tannins, phytosterols, diterpenes, and glycosides, which collectively enhance antibacterial and antioxidant activities [25,27,52,54]. These compounds are more effective in functionalizing the HAp surface, promoting stronger interactions with bacteria and ROS scavenging, and improving the overall activity. In contrast, *Punica granatum* peel extract is rich in polyphenols, flavonoids, tannins, anthocyanins, and organic acids, which also possess antibacterial and antioxidant properties but are less effective in comparison to the phytochemicals in *Citrus sinensis.* As confirmed by FTIR analysis, the higher concentration of active compounds in CS-HAp contribute to its better performance in antibiosis and ROS scavenging. These phytochemicals also play a key role in the formation and stabilization of the HAp nanorods during synthesis, enhancing their activity [25,40].

The HAp nanoparticles prepared through plant extract-mediated

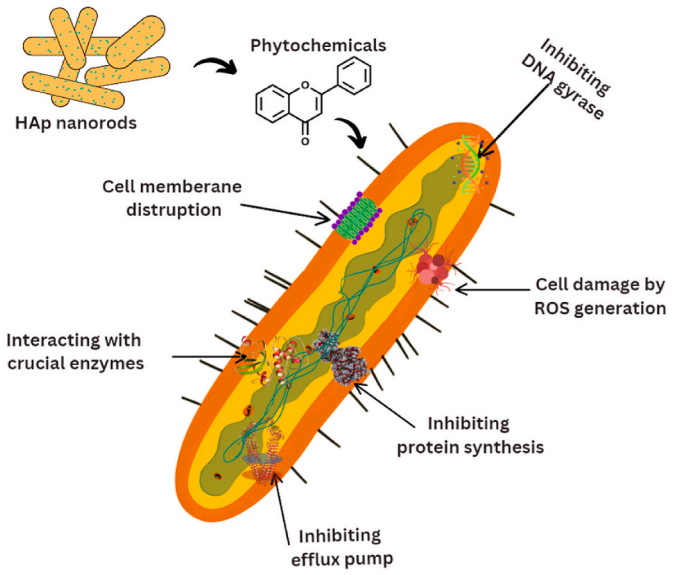

Fig. 6. The schematic of different pathways that are responsible for the effectiveness of HAp nanorods in inhibiting bacterial growth.

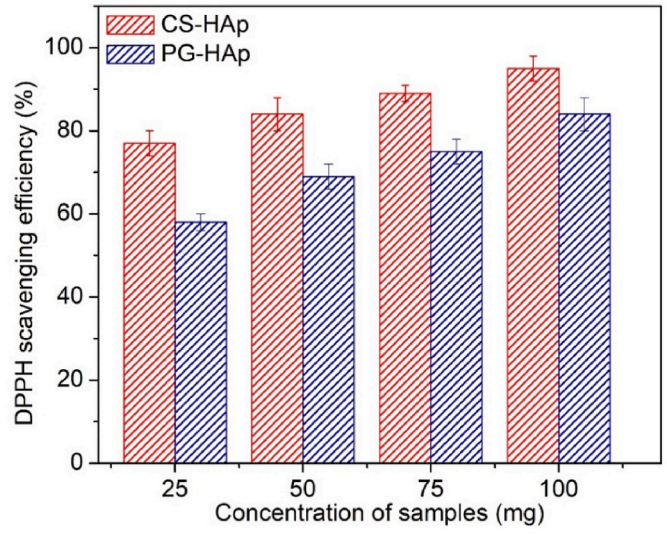

Fig. 7. Antioxidant activity of CS-HAp and PG-HAp samples.

Table 3
Recent studies on the development of HAp-based antioxidants and antibacterials using different plant extracts.

S. No	Plant extract	Morphology of HAp	Application in biomedicine	Authors
1	*Moringa oleifera*	Nanorods	Antibacterial and antifungal activity	[48]
2	*Curcuma longa tuber*	Nanorods	Antibacterial activity	[16]
3	Azadirachta indica & Coccinia grandis leaf	Nanorods	Antibacterial activity	[28]
4	*Opuntia ficus indica* fruit peel	Nanoparticles	Antibacterial and antifungal activity	[49]
5	Lavender and basil essential oils	Nanoparticles	Antibacterial activity	[57]
6	Piper betel leaf	Cylindrical-like nanoparticles	Antibacterial and antibiofilm activity	[50]
7	*Parkia biglobosa* pulp	Agglomerated nanoparticles	Antioxidant activity	[58]
8	Red beetroot	Nanocomposite	Antioxidant activity	[59]
9	*Terminalia Arjuna* bark	Spherical nanoparticles	Antioxidant activity	[60]
10	*Citrus sinensis* & *Punica granatum peel*	Nanorods	Antibacterial and Antioxidant activity	Present study

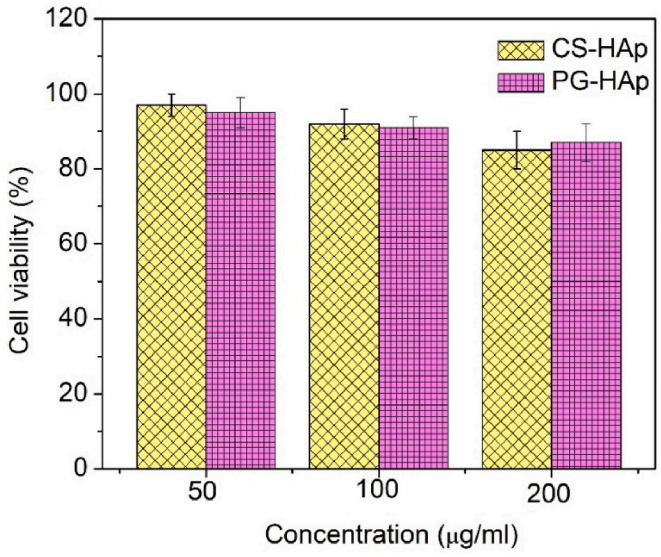

Fig. 8. Cell viability results of CS-HAp and PG-HAp at varying concentrations evaluated using the MTT assay.

green synthesis are widely used as antioxidants and antibacterials in biomedicine. Table 3 gives a summary of HAp nanoparticles obtained via a green approach using different plant extract and their characteristics. This table obviously supports our findings.

Fig. 8 shows the results of an MTT assay performed to evaluate the cell viability of CS-HAp and PG-HAp samples at concentrations of 50, 100, and 200 μg/mL. Both biomaterials exhibit high cell viability (>80 %) across all tested concentrations, indicating excellent cytocompatibility and minimal cytotoxic effects. At 50 μg/mL, cell viability is close to 100 % for both samples, while a slight decrease is observed at 100 μg/mL and 200 μg/mL. However, the values remain well above the 80 % threshold, confirming that both materials are biocompatible even at higher concentrations. Fig. 9 shows microscopic images of MG63 cells treated with synthesized HAp nanoparticles (CS-HAp and PG-HAp) at varying concentrations (50 μg/mL, 100 μg/mL, and 200 μg/mL), alongside untreated control cells. The control group demonstrates well-grown, intact MG63 cells forming a monolayer, characterized by their polygonal shape and visible cellular extensions. For the CS-HAp and PG-HAp treated groups, the images show that the cells maintain their morphology and integrity across all tested concentrations. The cells appear well spread with visible cellular extensions, resembling the control group. No significant changes in cell density or morphology were observed, indicating that the HAp nanoparticles did not cause toxicity or adverse effects on the cells. These findings align with the MTT assay results shown in Fig. 8 where cell viability remained greater than 80 % even at the maximum concentration of 250 μg/mL. The compatibility and retention of cell morphology in the treated samples demonstrate that both CS-HAp and PG-HAp nanoparticles are biocompatible and non-toxic to MG63 cells. This confirms the suitability of the synthesized HAp nanoparticles for biomedical applications due to their excellent cell compatibility and viability.

Fig. 10 shows live/dead cell staining of MG63 cells treated with CS-HAp and PG-HAp nanoparticles at different concentrations (50 μg/mL, 100 μg/mL, and 200 μg/mL) using a fluorescence assay. The green

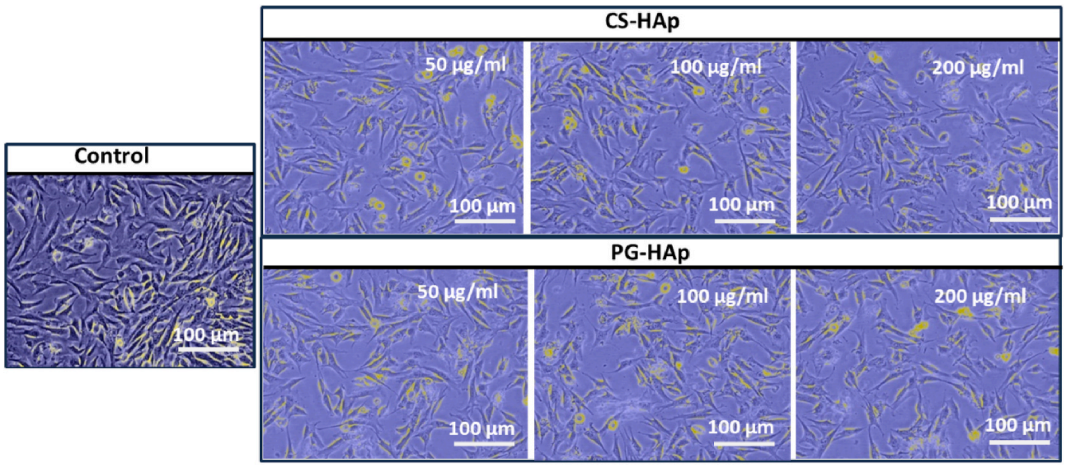

Fig. 9. Microscopic images of MG63 cells treated with CS-HAp and PG-HAp at different concentrations.

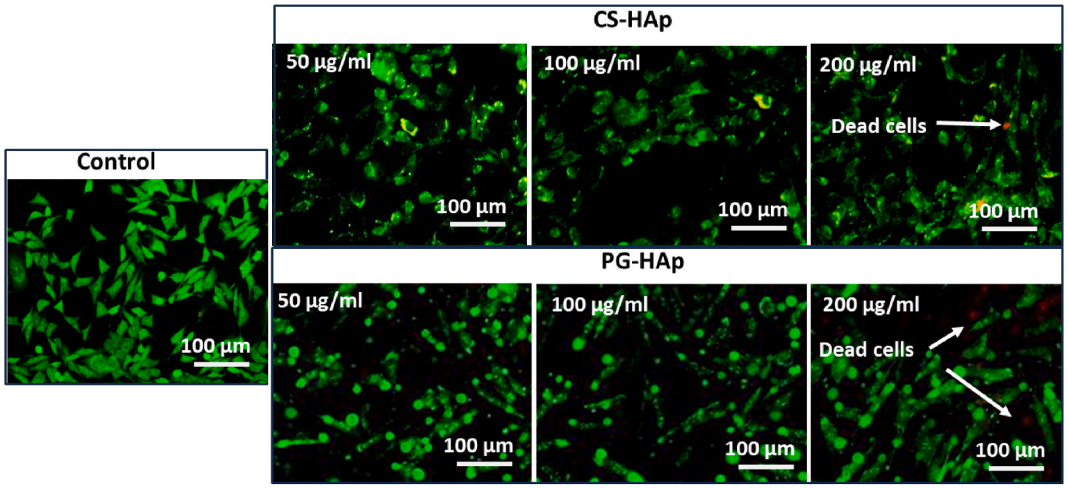

Fig. 10. Live/dead cell staining of MG63 cells treated with CS-HAp and PG-HAp at different concentrations using a fluorescence assay.

fluorescence indicates live cells, while red fluorescence represents dead cells. The control group shows a high density of live cells with no visible cell death. For both CS-HAp and PG-HAp treatments, the cells retain viability at lower concentrations (50 µg/mL and 100 µg/mL) with minimal dead cells observed. At the highest concentration (200 µg/mL), slight cytotoxicity is evident, as indicated by the presence of dead cells (red staining), though the majority of cells remain viable. The results confirm the biocompatibility of CS-HAp and PG-HAp nanoparticles, with cell viability remaining high across all concentrations. This assessment describes the appropriateness of CS-HAp and PG-HAp for biomedical applications, such as in bone tissue engineering, requiring biocompatibility to promote cell growth and viability [61].

The search for advanced functional biomaterials with functional properties is indeed a fascinating area in the field of nanotechnology and biomedicine [1,2]. Hydrothermal-assisted phyto-fabrication presented in the current study is one such method. This method not only enhances the functional properties of HAp nanorods but also promotes environmental sustainability. The significance of this study lies in its multifaceted approach to material synthesis, which addresses both environmental and biomedical challenges. By utilizing waste materials such as sea shells and fruit peels, the research promotes waste valorization and environmental sustainability [12,13]. Sea shells, primarily composed of calcium carbonate, serve as an abundant and cost-effective calcium source for HAp synthesis. The conversion of these waste materials into valuable biomedical products supports the principles of green chemistry and a circular economy [62,63]. Furthermore, the incorporation of natural extracts from *Citrus sinensis* and *Punica granatum peel* peels incorporate the bioactive compounds that enhance the antibacterial and antioxidant properties of the HAp nanorods, representing a significant advancement in material science and biomedical engineering. These properties are crucial for biomedical applications, particularly in bone tissue engineering, drug delivery systems, and antimicrobial coatings [13]. This study not only highlights the potential of waste materials in creating high-value biomedical products but also demonstrates the importance of integrating natural bioactive compounds to enhance the functional properties of synthetic materials [20]. This study also demonstrates how traditional waste materials can be transformed into high-value products with significant therapeutic benefits. The innovative approach of this research aligns with sustainable development goals and paves the way for future advancements in the development of eco-friendly and highly effective biomaterials.

4. Conclusion

This study demonstrates a successful sustainable synthesis of HAp nanorods from biowaste materials such as sea shells, *Citrus sinensis,* and *Punica granatum* fruit peels as calcium and templating agents. Hydrothermal treatment yielded uniform, well-defined HAp nanorods that possess excellent antibacterial and antioxidant properties as well as biocompatibility. Of the synthesized materials, *Citrus sinensis*-mediated

HAp (CS-HAp) showed better antibacterial and antioxidant activity than HAp mediated by *Punica granatum* (PG-HAp). Also, biocompatibility tests comprising MTT assay and live dead staining for cells showed a high cell viability, growth, and morphology integrity for MG63 cells treated with the synthesized HAp nanorods, thereby affirming the ability of these nanorods for biomedical applications. The influence of phytochemicals from *Citrus sinensis* and *Punica granatum* moieties not only controlled morphology but added value to the intrinsic bioactive properties of HAp. This research highlights the development of environment-friendly and high-efficiency biomaterials further intended for bone tissue engineering applications while upholding environmental sustainability through biowaste valorization.

CRediT authorship contribution statement

G. Suresh Kumar: Writing – original draft, Validation, Supervision. **K. Lalithambigai:** Writing – original draft, Validation, Supervision. **S. Ranjith Priyan:** Investigation, Formal analysis, Data curation. **Nguyen Van Minh:** Methodology, Formal analysis, Data curation. **M. Hariprasath:** Methodology, Investigation, Data curation. **G. Dineshkumar:** Methodology, Investigation, Data curation. **Srinivasan Ramalingam:** Writing – review & editing, Visualization. **Raji Atchudan:** Visualization, Formal analysis, Data curation. **Mohd Shkir:** Writing – review & editing, Funding acquisition.

Declaration of generative AI and AI-assisted technologies in the writing process

During the preparation of this work the authors used GRAMMERLY in order to enrich the English language. After using this tool, the authors reviewed and edited the content as needed and takes full responsibility for the content of the publication.

Declaration of competing interest

The authors declare that they have no known competing financial interests or personal relationships that could have appeared to influence the work reported in this paper.

Acknowledgements

The author from KKU extend their appreciation to the Deanship of Research and Graduate Studies at King Khalid University for funding this work through Large Research Project under grant number RGP2/465/46.

Appendix A. Supplementary data

Supplementary data to this article can be found online at https://doi.org/10.1016/j.ceramint.2025.07.161.

Data availability

The data that support the findings of this study are available from the corresponding author upon reasonable request.

References

[1] S.S. Ray, J. Bandyopadhyay, Nanotechnology-enabled biomedical engineering: current trends, future scopes, and perspectives, Nanotechnol. Rev. 10 (2021) 728–743, https://doi.org/10.1515/ntrev-2021-0052.
[2] M.Q. Chen, Recent advances and perspective of nanotechnology-based implants for orthopedic applications, Front. Bioeng. Biotechnol. 10 (2022), https://doi.org/10.3389/fbioe.2022.878257.
[3] J.G. Lyons, M.A. Plantz, W.K. Hsu, E.L. Hsu, S. Minardi, Nanostructured biomaterials for bone regeneration, Front. Bioeng. Biotechnol. 8 (2020), https://doi.org/10.3389/fbioe.2020.00922.
[4] Y. Hong, H. Fan, B. Li, B. Guo, M. Liu, X. Zhang, Fabrication, biological effects, and medical applications of calcium phosphate nanoceramics, in: Materials Science and Engineering R: Reports, 2010, pp. 225–242, https://doi.org/10.1016/j.mser.2010.06.010.
[5] M. Sadat-Shojai, M.T. Khorasani, E. Dinpanah-Khoshdargi, A. Jamshidi, Synthesis methods for nanosized hydroxyapatite with diverse structures, Acta Biomater. 9 (2013) 7591–7621, https://doi.org/10.1016/j.actbio.2013.04.012.
[6] G.S. Kumar, G. Karunakaran, E.K. Girija, E. Kolesnikov, N. Van Minh, M. V Gorshenkov, D. Kuznetsov, Size and morphology-controlled synthesis of mesoporous hydroxyapatite nanocrystals by microwave-assisted hydrothermal method, Ceram. Int. 44 (2018) 11257–11264.
[7] W. Zimmerli, Clinical presentation and treatment of orthopaedic implant-associated infection, J. Intern. Med. 276 (2014) 111–119, https://doi.org/10.1111/joim.12233.
[8] G.S. Kumar, R. Govindan, E.K. Girija, In situ synthesis, characterization and in vitro studies of ciprofloxacin loaded hydroxyapatite nanoparticles for the treatment of osteomyelitis, J. Mater. Chem. B 2 (2014) 5052–5060.
[9] M. Wang, T. Tang, Surface treatment strategies to combat implant-related infection from the beginning, J. Orthop.Transl. 17 (2019) 42–54, https://doi.org/10.1016/j.jot.2018.09.001.
[10] S. Ghasemi, S. Dabirian, F. Kariminejad, D.E. Koohi, M. Nemattalab, S. Majidimoghadam, E. Zamani, F. Yousefbeyk, Process optimization for green synthesis of silver nanoparticles using Rubus discolor leaves extract and its biological activities against multi-drug resistant bacteria and cancer cells, Sci. Rep. 14 (2024), https://doi.org/10.1038/s41598-024-54702-9.
[11] A.M. El Shafey, Green synthesis of metal and metal oxide nanoparticles from plant leaf extracts and their applications: a review, Green Process. Synth. 9 (2020) 304–339, https://doi.org/10.1515/gps-2020-0031.
[12] R. Veluswamy, G. Balasubramaniam, M. Natarajan, M. Krishnaswamy, B. A. Chinnappan, S. Nagarajan, B. Subramanian, D. Velauthapillai, Multifunctional and sustainable hydroxyapatite from natural products for biomedical and industrial applications - a comprehensive review, Sustain. Chem. Pharm. 41 (2024), https://doi.org/10.1016/j.scp.2024.101653.
[13] K. Alorku, M. Manoj, A. Yuan, A plant-mediated synthesis of nanostructured hydroxyapatite for biomedical applications: a review, RSC Adv. 10 (2020) 40923–40939, https://doi.org/10.1039/d0ra08529d.
[14] M. Chen, D. Jiang, D. Li, J. Zhu, G. Li, J. Xie, Controllable synthesis of fluorapatite nanocrystals with various morphologies: effects of pH value and chelating reagent, J. Alloys Compd. 485 (2009) 396–401, https://doi.org/10.1016/j.jallcom.2009.05.121.
[15] S.L. Bee, Z.A.A. Hamid, Hydroxyapatite derived from food industry bio-wastes: syntheses, properties and its potential multifunctional applications, Ceram. Int. 46 (2020) 17149–17175, https://doi.org/10.1016/j.ceramint.2020.04.103.
[16] G.S. Kumar, D. Muthu, G. Karunakaran, S. Karthi, E.K. Girija, D. Kuznetsov, Curcuma longa tuber extract mediated synthesis of hydroxyapatite nanorods using biowaste as a calcium source for the treatment of bone infections, J. Sol. Gel Sci. Technol. 86 (2018) 610–616.
[17] S.A. Singh, C. Vellapandian, D.D. Shah, T.J. Jayeoye, M.R. Chorawala, S. Singh, B. G. Prajapati, Valorised calcium-rich biomass from fish waste and eggshells in the fabrication of antibacterial scaffold for wound healing applications: a review, Waste Biomass Valorization 15 (2024) 1917–1941, https://doi.org/10.1007/s12649-023-02302-5.
[18] A.I. Adeogun, A.E. Ofudje, M.A. Idowu, S.O. Kareem, Facile development of nano size calcium hydroxyapatite based ceramic from eggshells: synthesis and characterization, Waste Biomass Valorization 9 (2018) 1469–1473, https://doi.org/10.1007/s12649-017-9891-3.
[19] G.S. Kumar, L. Sathish, R. Govindan, E.K. Girija, Utilization of snail shells to synthesise hydroxyapatite nanorods for orthopedic applications, RSC Adv 5 (2015) 39544–39548, https://doi.org/10.1039/C5RA04402B.
[20] U. Shanker, C.M. Hussain, M. Rani (Eds.), Handbook of Green and Sustainable Nanotechnology, Springer International Publishing, Cham, 2023, https://doi.org/10.1007/978-3-031-16101-8.
[21] R. Fernández-Penas, C. Verdugo-Escamilla, C. Triunfo, S. Gärtner, A. D'Urso, F. Oltolina, A. Follenzi, G. Maoloni, H. Cölfen, G. Falini, J. Gómez-Morales, A sustainable one-pot method to transform seashell waste calcium carbonate to osteoinductive hydroxyapatite micro-nanoparticles, J. Mater. Chem. B 11 (2023) 7766–7777, https://doi.org/10.1039/d3tb00856h.
[22] G. Borciani, T. Fischetti, G. Ciapetti, M. Montesissa, N. Baldini, G. Graziani, Marine biological waste as a source of hydroxyapatite for bone tissue engineering applications, Ceram. Int. 49 (2023) 1572–1584, https://doi.org/10.1016/j.ceramint.2022.10.341.
[23] P. Agalya, G. Suresh Kumar, R. Srinivasan, K.M. Prabu, G. Karunakaran, S. Cholan, E. Kolesnikov, M. Kim, Hydroxyapatite-based antibacterial bio-nanomaterials: an insight into the synthesis using mussel shell as a calcium source, physicochemical properties, and nanoindentation characteristics, Appl. Phys. A 127 (2021) 1–12.
[24] A.F. Ali, Z.A. Alrowaili, E.M. El-Giar, M.M. Ahmed, A.M. El-Kady, Novel green synthesis of hydroxyapatite uniform nanorods via microwave-hydrothermal route using licorice root extract as template, Ceram. Int. 47 (2021) 3928–3937, https://doi.org/10.1016/j.ceramint.2020.09.256.
[25] Z. Maqbool, W. Khalid, H.T. Atiq, H. Koraqi, Z. Javaid, S.K. Alhag, L.A. Al-Shuraym, D.M.D. Bader, M. Almarzuq, M. Afifi, A. Al-Farga, Citrus waste as source of bioactive compounds: extraction and utilization in health and food industry, Molecules 28 (2023), https://doi.org/10.3390/molecules28041636.
[26] S. Suri, A. Singh, P.K. Nema, Current applications of citrus fruit processing waste: a scientific outlook, Appl. Food Res. 2 (2022), https://doi.org/10.1016/j.afres.2022.100050.

[27] J. Singh, H.P. Kaur, A. Verma, A.S. Chahal, K. Jajoria, P. Rasane, S. Kaur, J. Kaur, M. Gunjal, S. Ercisli, R. Choudhary, M.R. Bozhuyuk, E. Sakar, N. Karatas, M. S. Durul, Pomegranate peel phytochemistry, pharmacological properties, methods of extraction, and its application: a comprehensive review, ACS Omega 8 (2023) 35452–35469, https://doi.org/10.1021/acsomega.3c02586.
[28] G.S. Kumar, S. Rajendran, S. Karthi, R. Govindan, E.K. Girija, G. Karunakaran, D. Kuznetsov, Green synthesis and antibacterial activity of hydroxyapatite nanorods for orthopedic applications, MRS Commun. 7 (2017) 183–188.
[29] C. Suryanarayana, M.G. Norton, X-Ray Diffraction, Springer US, Boston, MA, 1998, https://doi.org/10.1007/978-1-4899-0148-4.
[30] M. Othman, H.S. Loh, C. Wiart, T.J. Khoo, K.H. Lim, K.N. Ting, Optimal methods for evaluating antimicrobial activities from plant extracts, J. Microbiol. Methods 84 (2011) 161–166, https://doi.org/10.1016/j.mimet.2010.11.008.
[31] H.L. Bank, Assessment of islet cell viability using fluorescent dyes, Diabetologia 30 (1987), https://doi.org/10.1007/BF00275748.
[32] İ. Gulcin, S.H. Alwasel, DPPH radical scavenging assay, Processes 11 (2023) 2248, https://doi.org/10.3390/pr11082248.
[33] V. Devabharathi, K.S.G. Jagan, S.R. Priyan, T.N. Vidaarth, S. Surendhiran, Y.A. S. Khadar, K. Kandasamy, Rational design of NiO nanoflakes and porous GCN nanocomposite for synergic effectiveness on photocatalytic degradation of industry effluents and biological activity, Chem. Phys. Impact 8 (2024) 100637, https://doi.org/10.1016/j.chphi.2024.100637.
[34] M. Prakash, H.K. Rajan, M.N. Chandraprabha, S. Shetty, T. Mukherjee, S. Girish Kumar, Recent developments in green synthesis of hydroxyapatite nanocomposites: relevance to biomedical and environmental applications, Green Chem. Lett. Rev. 17 (2024), https://doi.org/10.1080/17518253.2024.2422409.
[35] Test method for evaluation of cytotoxicity of nanoparticulate materials in porcine kidney cells and human hepatocarcinoma cells. https://doi.org/10.1520/E2526-22, 2022.
[36] C.C. Coelho, L. Grenho, P.S. Gomes, P.A. Quadros, M.H. Fernandes, Nano-hydroxyapatite in oral care cosmetics: characterization and cytotoxicity assessment, Sci. Rep. 9 (2019) 11050, https://doi.org/10.1038/s41598-019-47491-z.
[37] S. Koutsopoulos, Synthesis and characterization of hydroxyapatite crystals: a review study on the analytical methods, J. Biomed. Mater. Res. 62 (2002) 600–612, https://doi.org/10.1002/jbm.10280.
[38] C. Ergun, Effect of Ti ion substitution on the structure of hydroxylapatite, J. Eur. Ceram. Soc. 28 (2008) 2137–2149, https://doi.org/10.1016/j.jeurceramsoc.2008.03.007.
[39] T.U. Doan Thi, T.T. Nguyen, Y.D. Thi, K.H. Ta Thi, B.T. Phan, K.N. Pham, Green synthesis of ZnO nanoparticles using orange fruit peel extract for antibacterial activities, RSC Adv. 10 (2020) 23899–23907, https://doi.org/10.1039/D0RA04926C.
[40] A.H. Hashem, E. Saied, O.M. Ali, S. Selim, S.K. Al Jaouni, F.M. Elkady, G.S. El-Sayyad, Pomegranate peel extract stabilized selenium nanoparticles synthesis: promising antimicrobial potential, antioxidant activity, biocompatibility, and hemocompatibility, Appl. Biochem. Biotechnol. 195 (2023) 5753–5776, https://doi.org/10.1007/s12010-023-04326-y.
[41] B.T.H. Otaviano, M. Sannomiya, R.S. de Queiroz, A.A.C. Sánchez, H.S. Freeman, L. E.R. Mendoza, J.L.S. Veliz, M.M.G. Leon, P. Leo, S.A. da Costa, S.M. da Costa, Natural dye extracted from pomegranate peel: physicochemical characterization, dyeing of cotton fabric, color fastness, and photoprotective properties, Fibers Polym. 24 (2023) 1321–1332, https://doi.org/10.1007/s12221-023-00138-3.
[42] O.E. Elazabawy, E.M. Attia, N.H. Shawky, A.M. Hyba, Eco-friendly orange peel extract as corrosion resistant for carbon steel's deterioration in petroleum formation water, Sci. Rep. 13 (2023) 21943, https://doi.org/10.1038/s41598-023-47916-w.
[43] G.S. Kumar, E.K. Girija, A. Thamizhavel, Y. Yokogawa, S.N. Kalkura, Synthesis and characterization of bioactive hydroxyapatite–calcite nanocomposite for biomedical applications, J. Colloid Interface Sci. 349 (2010) 56–62, https://doi.org/10.1016/j.jcis.2010.05.038.
[44] K. Naseem, M. Zia Ur Rehman, A. Ahmad, D. Dubal, T. AlGarni, Plant extract induced biogenic preparation of silver nanoparticles and their potential as catalyst for degradation of toxic dyes, Coatings 10 (2020) 1235, https://doi.org/10.3390/coatings10121235.
[45] B. Fultz, J. Howe, Transmission Electron Microscopy and Diffractometry of Materials, Springer Berlin Heidelberg, Berlin, Heidelberg, 2013, https://doi.org/10.1007/978-3-642-29761-8.
[46] S.A. Siddiqui, S. Singh, G.A. Nayik, Bioactive compounds from pomegranate peels - biological properties, structure–function relationships, health benefits and food applications – a comprehensive review, J. Funct.Foods 116 (2024) 106132, https://doi.org/10.1016/j.jff.2024.106132.
[47] S.S. Liew, W.Y. Ho, S.K. Yeap, S.A. Bin Sharifudin, Phytochemical composition and in vitro antioxidant activities of *Citrus sinensis* peel extracts, PeerJ 6 (2018) e5331, https://doi.org/10.7717/peerj.5331.
[48] V. Kalaiselvi, R. Mathammal, S. Vijayakumar, B. Vaseeharan, Microwave assisted green synthesis of Hydroxyapatite nanorods using *Moringa oleifera* flower extract and its antimicrobial applications, Int .J. Vet. Sci. Med. 6 (2018) 286–295, https://doi.org/10.1016/j.ijvsm.2018.08.003.
[49] D. Gopi, K. Kanimozhi, L. Kavitha, Opuntia ficus indica peel derived pectin mediated hydroxyapatite nanoparticles: synthesis, spectral characterization, biological and antimicrobial activities, Spectrochim. Acta Mol. Biomol. Spectrosc. 141 (2015) 135–143, https://doi.org/10.1016/j.saa.2015.01.039.
[50] M. Umesh, D.D. Choudhury, S. Shanmugam, S. Ganesan, M. Alsehli, A. Elfasakhany, A. Pugazhendhi, Eggshells biowaste for hydroxyapatite green synthesis using extract piper betel leaf - evaluation of antibacterial and antibiofilm activity, Environ. Res. 200 (2021) 111493, https://doi.org/10.1016/j.envres.2021.111493.
[51] C. Ragunath, L. Kousalya, R. Venkatachalam, S. Anitha, Green synthesis of hydroxyapatite nanoparticles from Wrightia tinctoria and its antibacterial activity, BioNanoScience 12 (2022) 723–730, https://doi.org/10.1007/s12668-022-01012-x.
[52] S. Shetty, P. Mahin-Syed-Ismail, S. Varghese, B. Thomas-George, P. Kandathil-Thajuraj, D. Baby, S. Haleem, S. Sreedhar, D. Devang-Divakar, Antimicrobial effects of citrus sinensis peel extracts against dental caries bacteria: an in vitro study, J. Clin. Exp. Dent. (2016), https://doi.org/10.4317/jced.52493, 0–0.
[53] M. Ayaz, F. Ullah, A. Sadiq, F. Ullah, M. Ovais, J. Ahmed, H.P. Devkota, Synergistic interactions of phytochemicals with antimicrobial agents: potential strategy to counteract drug resistance, Chem. Biol. Interact. 308 (2019) 294–303, https://doi.org/10.1016/j.cbi.2019.05.050.
[54] S. Malviya, Arvind, A. Jha, N. Hettiarachchy, Antioxidant and antibacterial potential of pomegranate peel extracts, J. Food Sci. Technol. 51 (2014) 4132–4137, https://doi.org/10.1007/s13197-013-0956-4.
[55] B. Khameneh, N.A.M. Eskin, M. Iranshahy, B.S. Fazly Bazzaz, Phytochemicals: a promising weapon in the arsenal against antibiotic-resistant bacteria, Antibiotics 10 (2021) 1044, https://doi.org/10.3390/antibiotics10091044.
[56] O.S. Nwozo, E.M. Effiong, P.M. Aja, C.G. Awuchi, Antioxidant, phytochemical, and therapeutic properties of medicinal plants: a review, Int. J. Food Prop. 26 (2023) 359–388, https://doi.org/10.1080/10942912.2022.2157425.
[57] D. Predoi, S.L. Iconaru, N. Buton, M.L. Badea, L. Marutescu, Antimicrobial activity of new materials based on lavender and Basil essential oils and hydroxyapatite, Nanomaterials 8 (2018) 291, https://doi.org/10.3390/nano8050291.
[58] S.A. Ibraheem, E.A. Audu, M. Jaafar, J.A. Adudu, J.T. Barminas, V. Ochigbo, A. Igunnu, S.O. Malomo, Novel pectin from Parkia biglobosa pulp mediated green route synthesis of hydroxyapatite nanoparticles, Surf. Interfaces 17 (2019) 100360, https://doi.org/10.1016/j.surfin.2019.100360.
[59] E.S. Bogya, M. Czikó, G. Szabó, R. Barabás, The red beetroot extract antioxidant activity and adsorption kinetics onto hydroxyapatite-based materials, J. Iran. Chem. Soc. 10 (2013) 491–503, https://doi.org/10.1007/s13738-012-0183-3.
[60] S. Husain, S. Sundari, R.K. Jain, S.R. Kumar, Green synthesis of terminalia arjuna-mediated hydroxyapatite nanoparticles, its morphological assessment and evaluation of cytotoxic and antioxidant properties: an In-vitro Study, J. Clin. Diagn. Res. (2023), https://doi.org/10.7860/JCDR/2023/59231.17659.
[61] G. Ciapetti, E. Cenni, L. Pratelli, A. Pizzoferrato, In vitro evaluation of cell/biomaterial interaction by MTT assay, Biomaterials 14 (1993) 359–364, https://doi.org/10.1016/0142-9612(93)90055-7.
[62] Y. Hou, A. Shavandi, A. Carne, A.A. Bekhit, T.B. Ng, R.C.F. Cheung, A.E.A. Bekhit, Marine shells: potential opportunities for extraction of functional and health-promoting materials, Crit. Rev. Environ. Sci. Technol. 46 (2016) 1047–1116, https://doi.org/10.1080/10643389.2016.1202669.
[63] N. Topić Popović, V. Lorencin, I. Strunjak-Perović, R. Čož-Rakovac, Shell waste management and utilization: mitigating organic pollution and enhancing sustainability, Appl. Sci. 13 (2023) 623, https://doi.org/10.3390/app13010623.